

Radial oscillations and stability of compact stars in Eddington-inspired Born-Infeld gravity

Y.-H. Sham, L.-M. Lin, P. T. Leung

*Department of Physics and Institute of Theoretical Physics,
The Chinese University of Hong Kong, Hong Kong SAR, China*

(Dated: February 7, 2022)

We study the hydrostatic equilibrium structure of compact stars in the Eddington-inspired Born-Infeld gravity recently proposed by Bañados and Ferreira [Phys. Rev. Lett. **105**, 011101 (2010)]. We also develop a framework to study the radial perturbations and stability of compact stars in this theory. We find that the standard results of stellar stability still hold in this theory. The frequency square of the fundamental oscillation mode vanishes for the maximum-mass stellar configuration. The dependence of the oscillation mode frequencies on the coupling parameter κ of the theory is also investigated. We find that the fundamental mode is insensitive to the value of κ , while higher-order modes depend more strongly on κ .

PACS numbers: 04.50.-h, 04.40.Dg, 98.80.-k

I. INTRODUCTION

General relativity (GR) has been the most successful and popular theory of gravity in the past century. From its classic predictions on the perihelion advance of Mercury and deflection of light, to the later predictions such as the orbital decay of the Hulse-Taylor binary pulsar due to gravitational-wave damping, GR has passed the experimental observations in these weak-field situations with flying colors. Testing the predictions of GR in strong-field situations, such as the final stage of binary black hole coalescence, will come soon from the detection of gravitational waves (see Ref. [1] for a review on experimental tests of GR).

Despite the great success of GR, the idea that GR may not be the correct theory to describe the Universe on cosmological scales is also gaining attention recently. This is due to the fact that, if GR is correct, we must then require the Universe to be dominated by some unknown component, called dark energy, in order to explain the accelerating expansion of the Universe. In the past decade, various alternative theories of gravity which deviate from GR on cosmological scales have been proposed in order to explain cosmological observations (see Ref. [2] for a recent review).

On the other hand, it is also well known that GR is not complete because of its prediction of spacetime singularities in the big bang and those inside black holes. It is generally believed that a consistent theory of quantum gravity is needed to resolve this issue. Recently, a new Eddington-inspired Born-Infeld (EiBI) theory of gravity was proposed by Bañados and Ferreira [3]. The appealing properties of this theory are that it is equivalent to GR in vacuum and can avoid the big bang singularity [3]. The theory differs from GR only in the presence of matter, and in particular the deviation becomes significant at high densities. It is thus reasonable to expect that compact stars may be the best astrophysical laboratories to test EiBI gravity. In fact, Pani *et al.* [4, 5] have recently studied the structure of compact stars in

EiBI gravity.

In this work, we report our investigation of compact stars in EiBI gravity. We first extend the work of Pani *et al.* [4, 5] by studying the static structure of compact stars in this theory using a large set of realistic equations of state (EOS). Furthermore, we develop a framework to study the radial perturbations and stability of these stars in this theory for the first time.

The plan of the paper is as follows: In Sec. II we briefly summarize EiBI gravity. In Sec. III we derive the equations for constructing static equilibrium stars in EiBI gravity. In Sec. IV we present the linearized equations for radial oscillations of compact stars. Section V presents the technique we use to employ realistic EOS models in this study. In Sec. VI we present our numerical results. Finally, our conclusions are summarized in Sec. VII. We use units where $G = c = 1$ unless otherwise noted.

II. EDDINGTON-INSPIRED BORN-INFELD GRAVITY

Here we briefly summarize the EiBI gravity proposed by Bañados and Ferreira [3]. The theory is based on the following action

$$S = \frac{1}{16\pi} \frac{2}{\kappa} \int d^4x \left(\sqrt{|g_{\mu\nu} + \kappa R_{\mu\nu}|} - \lambda \sqrt{-g} \right) + S_M[g, \Psi_M], \quad (1)$$

where $|f_{\mu\nu}|$ denotes the determinant of $f_{\mu\nu}$ and $g \equiv |g_{\mu\nu}|$. $R_{\mu\nu}$ represents the symmetric part of the Ricci tensor and is constructed solely from the connection $\Gamma_{\beta\gamma}^\alpha$. The matter action S_M is assumed to depend on the metric $g_{\mu\nu}$ and the matter field Ψ_M only. Furthermore, it can be shown that the action of Eq. (1) is equivalent to the Einstein-Hilbert action when $S_M = 0$, and hence the theory is identical to GR in vacuum [3].

The constants κ and λ are related to the cosmological constant by $\Lambda = (\lambda - 1)/\kappa$ such that, for small $\kappa R_{\mu\nu}$, the action [Eq. (1)] reduces to the Einstein-Hilbert action.

We shall fix $\lambda = 1$ in this work and treat κ as the only parameter of the theory. The constraints on κ based on solar observations [6], big bang nucleosynthesis and the existence of neutron stars [7] have been studied recently.

In this theory, the spacetime metric $g_{\mu\nu}$ and the connection $\Gamma_{\beta\gamma}^\alpha$ are treated as independent fields. The field equations are obtained by varying the action [Eq. (1)] with respect to $g_{\mu\nu}$ and $\Gamma_{\beta\gamma}^\alpha$ separately, and can be written as (with $\lambda = 1$) [3]

$$q_{\mu\nu} = g_{\mu\nu} + \kappa R_{\mu\nu}, \quad (2)$$

$$\sqrt{-q}q^{\mu\nu} = \sqrt{-g}g^{\mu\nu} - 8\pi\kappa\sqrt{-g}T^{\mu\nu}, \quad (3)$$

where $q_{\mu\nu}$ is an auxiliary metric compatible with the connection

$$\Gamma_{\beta\gamma}^\alpha = \frac{1}{2}q^{\alpha\sigma}(\partial_\gamma q_{\sigma\beta} + \partial_\beta q_{\sigma\gamma} - \partial_\sigma q_{\beta\gamma}), \quad (4)$$

and $q \equiv |q_{\mu\nu}|$. The stress-energy tensor $T^{\mu\nu}$ satisfies the same conservation equations as in GR:

$$\nabla_\mu T^{\mu\nu} = 0, \quad (5)$$

where the covariant derivative refers to the metric $g_{\mu\nu}$.

III. STATIC EQUILIBRIUM CONFIGURATIONS

A. Basic equations

The structure of compact stars in EiBI theory was first studied by Pani *et al.* [4, 5]. Here we present our formulation which uses different variables, and hence leads to a different set of differential equations which resemble more closely the corresponding equations in GR. For a static and spherically symmetric spacetime, the spacetime metric $g_{\mu\nu}$ and the auxiliary metric $q_{\mu\nu}$ are taken to be

$$g_{\mu\nu}dx^\mu dx^\nu = -e^{\phi(r)}dt^2 + e^{\lambda(r)}dr^2 + f(r)d\Omega^2, \quad (6)$$

$$q_{\mu\nu}dx^\mu dx^\nu = -e^{\beta(r)}dt^2 + e^{\alpha(r)}dr^2 + r^2d\Omega^2. \quad (7)$$

Note that the gauge freedom has been used to set $q_{\theta\theta} = r^2$. The matter is assumed to be a perfect fluid and is described by the stress-energy tensor

$$T^{\mu\nu} = (\epsilon + P)u^\mu u^\nu + Pg^{\mu\nu}, \quad (8)$$

where ϵ and P are the energy density and pressure of the fluid, respectively. The four-velocity of the fluid u^μ is given by $u^\mu = (e^{-\phi/2}, 0, 0, 0)$ because of the time and spherical symmetry of the spacetime. The stress-energy tensor is then simplified to

$$T_t^t = -\epsilon, \quad T_r^r = T_\theta^\theta = T_\varphi^\varphi = P. \quad (9)$$

Note that the indices of $T^{\mu\nu}$ are raised with the spacetime metric $g_{\mu\nu}$.

From Eq. (3), one can obtain the relations

$$e^\beta = e^\phi b^3 a^{-1}, \quad e^\alpha = e^\lambda ab, \quad (10)$$

where $a \equiv \sqrt{1 + 8\pi\kappa\epsilon}$ and $b \equiv \sqrt{1 - 8\pi\kappa P}$. In addition, $f(r)$ is found to be

$$f(r) = \frac{r^2}{ab}. \quad (11)$$

The field equations of Eq. (2) reduce to the following two independent equations

$$\frac{1}{\kappa} \left(2 + \frac{a}{b^3} - \frac{3}{ab} \right) = \frac{2}{r^2} - \frac{2}{r^2}e^{-\alpha} + \frac{2}{r}e^{-\alpha}\alpha', \quad (12)$$

$$\frac{1}{\kappa} \left(\frac{1}{ab} + \frac{a}{b^3} - 2 \right) = -\frac{2}{r^2} + \frac{2}{r^2}e^{-\alpha} + \frac{2}{r}e^{-\alpha}\beta', \quad (13)$$

where primed quantities denote partial derivatives with respect to r . The conservation of the stress-energy tensor [Eq. (5)] gives

$$\phi' = -\frac{2P'}{P + \epsilon}. \quad (14)$$

Eqs. (12) - (14) can be combined to obtain the following two first-order differential equations:

$$\begin{aligned} \frac{dP}{dr} = & - \left[\frac{1}{2\kappa} \left(\frac{1}{ab} + \frac{a}{b^3} - 2 \right) r + \frac{2m}{r^2} \right] \left[1 - \frac{2m}{r} \right]^{-1} \\ & \times \left[\frac{2}{\epsilon + P} + \frac{\kappa}{2} \left(\frac{3}{b^2} + \frac{1}{a^2 c_s^2} \right) \right]^{-1}, \end{aligned} \quad (15)$$

$$\frac{dm}{dr} = \frac{1}{4\kappa} \left(2 - \frac{3}{ab} + \frac{a}{b^3} \right) r^2, \quad (16)$$

where the speed of sound c_s is calculated by $c_s^2 = dP/d\epsilon$. The function $m(r)$ is defined by

$$e^{-\lambda} = \left(1 - \frac{2m}{r} \right) ab. \quad (17)$$

With a given EOS $P = P(\epsilon)$, the structure of a hydrostatic equilibrium star in EiBI gravity is obtained by solving Eqs. (15) and (16). By expanding a and b in series of κ , it can be shown that these equations reduce to the corresponding structure equations in GR when $\kappa \rightarrow 0$ (see, e.g., Ref. [8]).

B. Boundary conditions and numerical scheme

To construct a static compact star with a given EOS, we first integrate Eqs. (15) and (16) by specifying the central density ϵ_c , and hence the central pressure P_c , and setting $m(0) = 0$. The radius of the star R is defined by the condition $P(R) = 0$. As discussed above, EiBI gravity is equivalent to GR in vacuum. Hence, the interior solution should match smoothly to the Schwarzschild solution at the stellar surface. It can be checked that the required conditions are $\epsilon(R) = P(R) = 0$ and hence $a(R) =$

$b(R) = 1$. We then have $e^{-\alpha(R)} = e^{-\lambda(R)} = (1 - 2M/R)$, where $M \equiv m(R)$ is the mass of the star. We also require that $e^{\beta(R)} = e^{\phi(R)} = (1 - 2M/R)$. The function $\beta(r)$, and hence $\phi(r)$ because of Eq. (10), can now be obtained by integrating Eq. (13) backward from the surface to the center. We have now completed the interior solution of the star. It should be noted that the appearance of the terms $a = \sqrt{1 + 8\pi\kappa\epsilon}$ and $b = \sqrt{1 - 8\pi\kappa P}$ in the theory imposes the following conditions (see also Refs. [4, 5]):

$$8\pi\kappa P_c < 1, \quad \text{for } \kappa > 0, \quad (18)$$

$$8\pi|\kappa|\epsilon_c < 1, \quad \text{for } \kappa < 0. \quad (19)$$

IV. RADIAL OSCILLATIONS

A. Equations for radial perturbations

In order to check the stability of compact stars constructed in EiBI gravity, we need to study the radial oscillation modes of these stars. The corresponding study in GR was first performed by Chandrasekhar almost fifty years ago [9] (see also Ref. [10] for a more recent study). Here we shall derive an eigenvalue equation [see Eq. (30) below] which allows us to obtain the frequencies of radial oscillation modes of compact stars in EiBI gravity. Since the calculation is somewhat tedious, we shall thus only outline the main steps of the derivation in the following.

We assume that the static background star is perturbed radially so that spherical symmetry is maintained. The spacetime metric can still be written as Eq. (6), but now the components g_{tt} and g_{rr} depend on both r and t (see, e.g., Ref. [11]):

$$g_{\mu\nu}dx^\mu dx^\nu = -e^{\phi(t,r)}dt^2 + e^{\lambda(t,r)}dr^2 + f(r)d\Omega^2. \quad (20)$$

The auxiliary metric $q_{\mu\nu}$ takes the form

$$q_{\mu\nu}dx^\mu dx^\nu = -e^{\beta(t,r)}dt^2 + e^{\alpha(t,r)}dr^2 + 2\eta(t,r)dtdr + r^2d\Omega^2, \quad (21)$$

where the tr component $[q_{tr} \equiv \eta(t, r)]$ is in general nonzero. The four-velocity of the fluid is now given by

$$u^\mu = (-e^{\phi/2}, e^{-\phi/2}\dot{\xi}, 0, 0), \quad (22)$$

where ξ is the Lagrangian displacement and $\dot{\xi} \equiv \partial\xi/\partial t$. To linear order in ξ , the nonvanishing components of the stress-energy tensor are

$$T_t^t = -\epsilon, \quad T_r^r = T_\theta^\theta = T_\varphi^\varphi = P, \quad (23)$$

$$T_t^r = -(\epsilon_0 + P_0)\dot{\xi}, \quad (24)$$

where ϵ_0 and P_0 refer to the energy density and pressure of the unperturbed static background, respectively. It should be noted that Eqs. (3) and (24) imply that the auxiliary metric function $\eta(t, r)$ is in general nonzero even though $g_{tr} = 0$.

We now consider small radial perturbations on the static background solution such that $F(t, r) = F_0(r) + \delta F(t, r)$, where F stands for any metric or fluid variable and F_0 is its background solution. We shall derive the linearized field and matter equations by retaining terms only of first order in ξ and δF . To obtain the oscillation mode frequencies, we assume a time dependence $e^{i\omega t}$ for all the perturbed quantities. Eqs. (2) and (3) can then be reduced to the following equations

$$\delta\alpha = -\frac{e^\alpha}{r}\chi, \quad (25)$$

$$\chi' = -r^2 Q_2 \delta\epsilon, \quad (26)$$

$$\delta\beta = \delta\phi - 4\pi\kappa \left[\frac{3\delta P}{1 - 8\pi\kappa P} + \frac{\delta\epsilon}{1 + 8\pi\kappa\epsilon} \right], \quad (27)$$

$$\delta\beta' = -\frac{e^\alpha}{r} Q_3 \chi' - \frac{e^\alpha}{r} Q_4 \chi, \quad (28)$$

where $\chi \equiv r^2(\epsilon + P)Q_1\xi$. In the above, physical quantities without “ δ ” are evaluated on the static background. The functions Q_i are given explicitly in Appendix A. On the other hand, the linearized conservation equation (5) becomes

$$e^{\lambda-\phi}(\epsilon + P)\omega^2\chi = \delta P' + \frac{1}{2}(\epsilon + P)\delta\phi' + \frac{1}{2}(1 + c_s^2)\phi'\delta P. \quad (29)$$

Combining the above linearized equations, we obtain our eigenvalue equation for determining the radial oscillation modes

$$\chi'' = -W_1\chi - W_2\chi', \quad (30)$$

where the functions W_1 and W_2 depend only on the background quantities and the frequency square ω^2 (see Appendix A for their expressions).

B. Boundary conditions and numerical scheme

The Lagrangian displacement ξ must vanish at the center due to spherical symmetry. From the definition of χ , this condition is equivalent to

$$\chi(0) = 0. \quad (31)$$

At the stellar surface, the appropriate boundary condition is that the Lagrangian variation of the pressure vanishes ($\delta P = 0$). It can be shown from Eq. (26), with the conditions $P(R) = \epsilon(R) = 0$, that the boundary condition is equivalent to the requirement that the displacement ξ is finite at the surface. From the definition of χ , the boundary condition is thus equivalent to

$$\chi(R) = 0. \quad (32)$$

To find ω^2 numerically, the shooting method is applied. We first decompose Eq. (30) into two first-order differential equations for χ and χ' . In practice, we choose a trial

eigenvalue ω^2 and start our numerical integration at a point near the center. Note that the regularity condition of χ implies that $\chi \sim r^3$ for small r . We integrate up to the stellar surface and check whether Eq. (32) is satisfied. The eigenvalue is obtained if the trial ω^2 can satisfy the boundary condition. Otherwise, the integration is repeated with a different trial ω^2 .

V. EQUATION OF STATE

In constructing a compact star, one has to specify an EOS model that gives the relation between P and ϵ . Although polytropic EOSs are often used in compact star simulations, they are oversimplified and cannot reflect the complexity of nuclear matter. On the other hand, realistic EOS models are usually presented in tabulated forms and one needs in general to perform numerical interpolations in the study. Alternatively, one can also use piecewise polytropic models to fit many tabulated EOSs in different density regions [12].

The above two techniques in general work well for studying compact stars in GR. However, we found that they are not good enough for studying the oscillation modes of compact stars in EiBI gravity. The reason is that the eigenvalue equation [Eq. (30)] involves the derivative c'_s , which is proportional to $d^2P/d\epsilon^2$. It is noted that, for the corresponding study in GR, one only needs to calculate $dP/d\epsilon$ [10]. In order to apply realistic EOS models in our study, we use smooth analytic functions to model the tabulated EOS models so that the second derivative $d^2P/d\epsilon^2$ can be computed analytically, and hence numerical errors can be reduced. In particular, we use the following analytical representation suggested by Haensel and Potekhin [13]:

$$\begin{aligned} \tilde{P} = & \frac{a_1 + a_2\tilde{\epsilon} + a_3\tilde{\epsilon}^3}{1 + a_4\tilde{\epsilon}} f(a_5(\tilde{\epsilon} - a_6)) \\ & + (a_7 + a_8\tilde{\epsilon}) f(a_9(a_{10} - \tilde{\epsilon})) \\ & + (a_{11} + a_{12}\tilde{\epsilon}) f(a_{13}(a_{14} - \tilde{\epsilon})) \\ & + (a_{15} + a_{16}\tilde{\epsilon}) f(a_{17}(a_{18} - \tilde{\epsilon})), \end{aligned} \quad (33)$$

where $\tilde{P} = \log(P/\text{dyn cm}^{-2})$, $\tilde{\epsilon} = \log(\epsilon/\text{g cm}^{-3})$, and $f(x) = 1/(e^x + 1)$. The 18 constants a_i are fitting parameters. For a given tabulated EOS, we use the Levenberg-Marquardt method [14] to determine the set of parameters a_i that best fits the EOS data points. In this work, we consider the following eight realistic EOSs: model A [15], model APR [16], model BBB2 [17], model C [18], model FPS [19], model SLy4 [20], model UU [21, 22], and model WS [19, 21].

To show the accuracy of our analytical representations of the tabulated EOS, we plot in Fig. 1 the analytical fits to the BBB2 (solid line) and FPS (dashed line) EOS models. The original EOS data points are denoted by the cross (BBB2) and plus (FPS) symbols in the figure. It is seen from the figure that the analytic fits match the data points of the tabulated EOSs very well. Furthermore, we

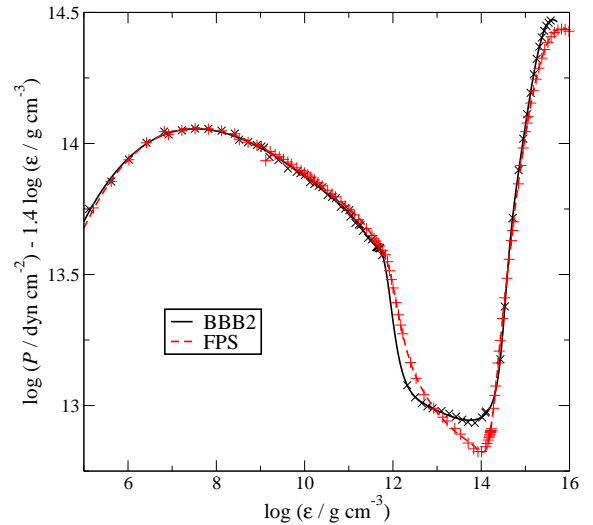


FIG. 1: Plot of the analytic fit of the BBB2 and FPS models. The crosses and pluses represent the data points in the EOS tables and the lines are the analytic fit functions (see also Fig. 2 of Ref. [13]).

find that the standard deviations between the original EOS data and fitting data points are in general of the order 10^{-2} or less for all the EOS models.

VI. RESULTS

In this section, we shall construct static equilibrium compact stars and study their stability in EiBI gravity. As discussed in Sec. II, the free parameter of the theory is κ . For $\kappa = 0$, the theory is equivalent to GR. On the other hand, the more interesting case is $\kappa > 0$ because it is the regime where novel properties of EiBI gravity exist. In this regime, the theory leads to a nonsingular cosmological model [3] and the existence of pressureless stars [4, 5]. In this work, we shall consider three different values of κ defined by $8\pi\kappa\epsilon_0 = -0.1, 0, 0.1$, where $\epsilon_0 = 10^{15} \text{g cm}^{-3}$. These values of κ are consistent with the recent constraint set by the existence of neutron stars as proposed in Ref. [7], though it should be noted that we use units where $G = c = 1$ in this work.

To demonstrate the stability of compact stars in EiBI gravity, we show in Figs. 2 (a)-2(d) the numerical results for the APR, BBB2, FPS, and SLy4 EOS models. For each case, we plot the gravitational mass M and the frequency square ω^2 of the fundamental oscillation mode as a function of the central density ϵ_c in the upper and lower panels, respectively. The circle on each $M-\epsilon_c$ curve corresponds to the maximum-mass stellar configuration. It is seen from the figures that the $M-\epsilon_c$ relation in EiBI gravity is qualitatively similar to that in GR. The stellar mass increases with the central density until it reaches a maximum. In GR, it is known that the mode frequency passes through zero at the central density corresponding

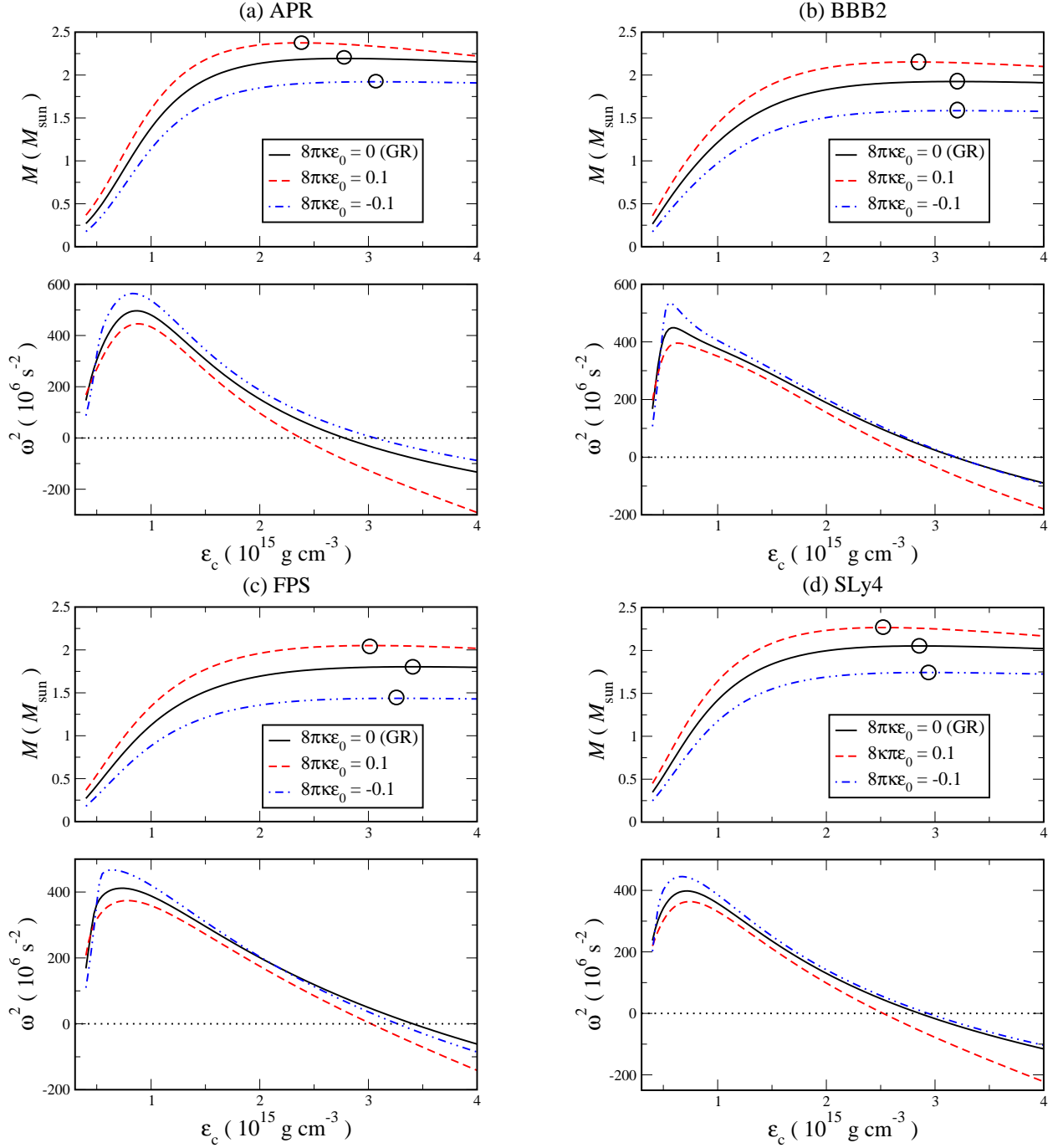


FIG. 2: Gravitational mass M and fundamental mode frequency square ω^2 plotted against the central density ϵ_c for the four EOS models: (a) APR, (b) BBB2, (c) FPS and (d) SLy4. Three different values of κ are considered. The circle on each M - ϵ_c curve corresponds to the maximum-mass configuration.

to the maximum-mass configuration. This critical density corresponds to the onset of dynamical instability in the sense that stellar models beyond this critical point are unstable against radial perturbations. Our results show that this property is also true in EiBI gravity. We see that ω^2 also passes through zero at the maximum-mass configuration in EiBI gravity. For a given EOS, stellar models with central densities less than the critical den-

sity are stable because the fundamental mode frequency square $\omega^2 > 0$. We have thus demonstrated the stability of compact stars in EiBI gravity.

For a given EOS model, we see that a negative value of κ in general decreases the maximum mass of a neutron star compared to the case of GR. On the other hand, for a positive value of κ , EiBI gravity can lead to a much larger maximum mass. As pointed out in Ref. [5], this has

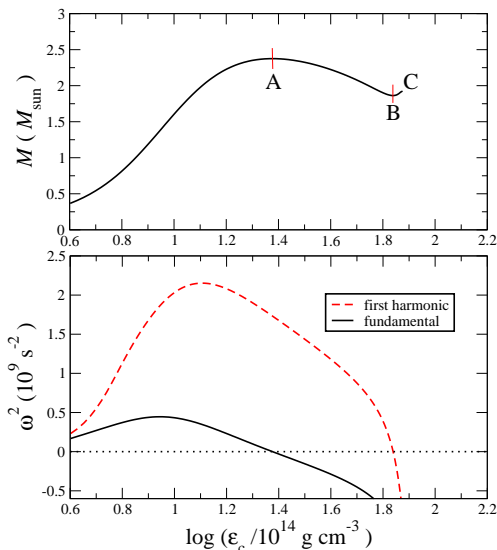


FIG. 3: Upper panel: Gravitational mass as a function of the central density for compact stars modeled by the APR EOS and $8\pi\kappa\epsilon_0 = 0.1$. The curve terminates at the point C where Eq. (18) is violated. Lower panel: Frequency square of the fundamental (solid line) and first harmonic (dashed line) modes as a function of the central density.

TABLE I: Mass and radius of the maximum-mass stellar configuration for each EOS model. Mass M_{max} is expressed in solar mass units, and radius R is expressed in km.

	$8\pi\kappa\epsilon_0 = -0.1$		$8\pi\kappa\epsilon_0 = 0$		$8\pi\kappa\epsilon_0 = 0.1$	
EOS	M_{max}	R	M_{max}	R	M_{max}	R
A	1.240	7.65	1.656	8.21	1.916	8.98
APR	1.922	9.23	2.191	9.82	2.375	10.47
BBB2	1.585	8.83	1.922	9.36	2.152	10.03
C	1.488	9.29	1.838	9.68	2.089	10.33
FPS	1.434	8.60	1.800	9.10	2.050	9.79
SLy4	1.744	9.33	2.052	9.86	2.268	10.51
UU	1.932	9.08	2.196	9.67	2.371	10.34
WS	1.495	8.90	1.845	9.42	2.094	10.05

the interesting implication that some softer EOS models, which are ruled out in GR by the recent discovery of a neutron star with $M \approx 1.97M_\odot$ [23], would be revived in EiBI gravity. For example, the maximum mass of a neutron star for the FPS EOS in GR is $M = 1.8M_\odot$. However, it can increase to $2M_\odot$ in EiBI gravity for the case $8\pi\kappa\epsilon_0 = 0.1$. In Table I, we list the mass and radius of the maximum-mass configuration for each EOS model we consider in this work. Furthermore, we list the mass and fundamental mode frequency as a function of the central density for each EOS model in Appendix B.

It is recalled that Eqs. (18) and (19) must be fulfilled in order to construct compact stars in EiBI gravity. In the upper panel of Fig. 3 we plot M against ϵ_c for compact

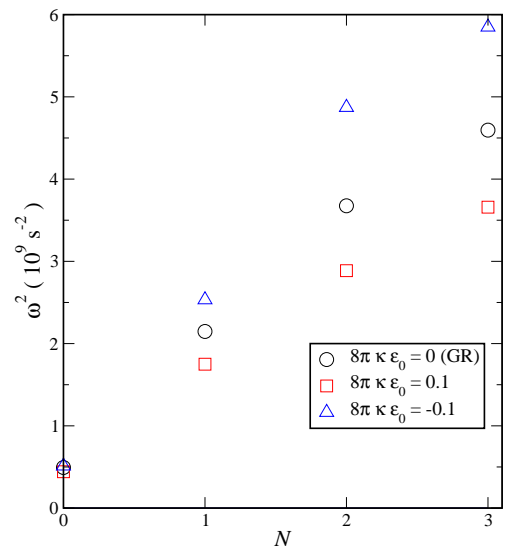


FIG. 4: Frequency square ω^2 plotted against the number of nodes N in the mode eigenfunctions for compact stars modeled by the APR EOS. The stellar mass $M = 1.25M_\odot$ is fixed.

stars modeled by the APR EOS and $8\pi\kappa\epsilon_0 = 0.1$ again, but now the central density is extended to the point C where Eq. (18) is violated. In the lower panel, we plot the frequency square ω^2 of the fundamental and first harmonic modes against ϵ_c . As we have seen in Fig. 2 (a), the fundamental mode becomes unstable at the first critical point A. However, we now also see that there exists a second critical point B at higher densities. Figure 3 shows clearly that it is the first harmonic that changes stability at this point. The stellar models from B to C are still unstable even though $dM/d\epsilon_c > 0$ in this range. Similar to standard neutron stars in GR [8], we have thus seen that the criterion $dM/d\epsilon_c > 0$ also does not guarantee stellar stability in EiBI gravity.

To end this section, we study how the value of κ would affect the oscillation mode frequencies. Since the gravitational mass of a compact star can usually be measured more accurately than its radius (see Ref. [24] for a review on neutron star observations), we shall thus consider the oscillation modes of compact star models with a given mass for different values of κ . In Fig. 4, we plot the frequency square ω^2 against the number of nodes N in the mode eigenfunctions. The stellar models have the same mass $M = 1.25M_\odot$ and are described by the same APR EOS. Three different cases $8\pi\kappa\epsilon_0 = -0.1, 0, 0.1$ are considered as before. Note that the fundamental mode has zero nodes, and we see from the figure that the frequency of this mode is insensitive to the value of κ . On the contrary, higher-order modes (i.e., modes with larger values of N) depend more sensitively on the value of κ . In particular, a positive (negative) value of κ would decrease (increase) the frequencies of higher-order modes. While we only show the results of three different values of κ in Fig. 4, we have seen that this property is in general true for other values.

Finally, we note that the sensitivity of the frequencies of higher-order modes on κ may be understood heuristically by noting that, in the nonrelativistic limit of EiBI gravity, the standard Poisson equation in Newtonian theory is modified by having an extra source term of the form $\kappa \nabla^2 \rho$, where ρ is the mass density [3]. A larger variation of density perturbation, which is the case for higher-order modes, would then lead to a larger difference in the stellar dynamics comparing to the Newtonian results. On the other hand, the fundamental mode eigenfunction has no node and is monotonically increasing in the star. Hence, the magnitude of $\nabla^2 \delta \rho$ (with $\delta \rho$ being the density perturbation associated to the mode) should in general be smaller than those of higher-order modes. This makes the frequency of the fundamental mode not so sensitive to κ . We believe that this property is also true in our fully relativistic study, as shown in Fig. 4.

VII. CONCLUSION

In this paper, we have studied the equilibrium structure of compact stars in EiBI gravity using a set of eight realistic EOS models. Our formulation of the structure equations is different from the recent works of Pani *et al.* [4, 5] in such a way that the resulting differential equations resemble more closely the corresponding equations in GR. We solved the structure equations numerically and found that the maximum mass of a neutron star can be larger than that in GR when the parameter κ in EiBI gravity is positive. This implies that softer EOS models, which are ruled out in GR by the recent discovery of a neutron star with mass nearly $2M_\odot$, would be revived in EiBI gravity [5].

We have also developed a theory of radial perturbation and studied the stability of compact stars in EiBI gravity by calculating the oscillation mode frequency square ω^2 for the first time. In contrast to the situation in GR, since the oscillation equation in EiBI gravity involves the second derivative $dP^2/d\epsilon^2$, we found that using standard techniques such as numerical interpolation or piecewise polytropic representation [12] to handle realistic EOS tables in the calculation would not produce reliable numerical results. This is because the data points in standard EOS tables are usually not dense enough to allow an accurate calculation of $dP^2/d\epsilon^2$. We thus followed Ref. [13] and used an 18-parameter analytic representation to model the EOS in our calculation. It should, however, be emphasized that the analytic fitting is not fundamentally essential to our stability analysis. It is employed in this work in order to improve numerical accuracy only.

We find that the standard results of stellar stability still hold in EiBI gravity. For a sequence of stars modeled by the same EOS, we found that the fundamental mode frequency square passes through zero at the central density corresponding to the maximum-mass configuration. Similar to the analysis of compact stars in GR, this point marks the onset of instability. Stellar models with

central densities less than the critical point are stable because $\omega^2 > 0$. Furthermore, we also found that the criterion $dM/d\epsilon_c > 0$ does not guarantee stellar stability.

We have also studied the effects of the parameter κ on the oscillation modes. For a fixed stellar mass, we found that the fundamental mode frequency is insensitive to the value of κ . On the contrary, the frequencies of higher-order modes depend strongly on κ . In particular, a positive (negative) value of κ would decrease (increase) the frequencies of higher-order modes. Our results thus suggest that the detection of higher-order radial oscillation modes might provide useful constraints on the value of κ if they could be excited to large amplitudes. Of course, in reality oscillation modes could in general be excited to large amplitudes only in some catastrophic situations such as core collapse supernovae. However, those catastrophic events are in general highly nonspherical, and hence nonradial oscillation modes could become more relevant. Studying nonradial oscillations of compact stars and the corresponding gravitational wave signals would be a natural extension of our present work. We hope to return to this issue in the future and study whether the gravitational wave signals emitted by compact stars could be used to constrain EiBI gravity.

Appendix A: List of functions

Here we present the expressions for the various functions Q_i and W_i used in Sec. IV:

$$Q_1 = \frac{8\pi}{a^2} \left[1 + \kappa e^{-\alpha} \left(\frac{\beta'}{r} - \frac{\alpha' \beta'}{4} + \frac{\beta'^2}{4} + \frac{\beta''}{2} \right) \right]$$

$$Q_2 = 6\pi \left[\frac{a^2 + 3b^2}{3a^3b^3} + \frac{a}{b^3} \left(\frac{1}{b^2} - \frac{1}{a^2} \right) c_s^2 \right], \quad (A1)$$

$$Q_3 = 2\pi \left[\frac{1}{a^2} \left(\frac{a}{b^3} - \frac{1}{ab} \right) + \frac{c_s^2}{b^2} \left(\frac{3a}{b^3} + \frac{1}{ab} \right) \right], \quad (A2)$$

$$Q_4 = \frac{1}{r} + \beta' + 16\pi e^{\alpha-\beta} \kappa \frac{P + \epsilon \omega^2}{a^2 Q_1}, \quad (A3)$$

$$Q_5 = 4\pi \kappa \left[\frac{3c_s^2}{b^2} + \frac{1}{a^2} \right], \quad (A4)$$

$$Q_6 = 4\pi \kappa \left(\frac{6c_s}{b^2} c_s' - \frac{6c_s^2}{b^3} b' - \frac{2}{a^3} a' \right), \quad (A5)$$

$$Q_7 = r e^\alpha Q_3 + Q_6 - Q_5 \left(\frac{2}{r} + \frac{Q_2'}{Q_2} \right), \quad (A6)$$

$$W_1 = Q_2 \left[\frac{e^{\lambda-\phi} \omega^2}{Q_1} + \frac{r}{2} (P + \epsilon) e^\alpha Q_4 \right] \times \left[c_s^2 + \frac{1}{2} (P + \epsilon) Q_5 \right]^{-1}, \quad (A7)$$

$$W_2 = \left[c_s^2 + \frac{1}{2} (P + \epsilon) Q_5 \right]^{-1} \left[2c_s c_s' + \frac{1}{2} (1 + c_s^2) \phi' \right]$$

$$-c_s^2 \left(\frac{2}{r} + \frac{Q'_2}{Q_2} \right) + \frac{1}{2}(P + \epsilon)Q_7 \Big]. \quad (\text{A8})$$

Appendix B: Numerical data

In this appendix, we provide the numerical data for the gravitational mass M and fundamental mode frequency square ω^2 . In Tables II to IX, we list M and ω^2 as a function of the central density ϵ_c for three different parameters: $8\pi\kappa\epsilon_0 = -0.1, 0, 0.1$. In the GR limit ($\kappa = 0$), we have checked that stellar models obtained by using our analytical representations of the EOS and those by the original EOS data (with numerical interpolation) agree very well. For example, the central densities of the maximum-mass configurations obtained by the two methods are in general different by about 1% only.

TABLE II: Model A.

	$8\pi\kappa\epsilon_0 = -0.1$		$8\pi\kappa\epsilon_0 = 0$		$8\pi\kappa\epsilon_0 = 0.1$	
ϵ_c	M	ω^2	M	ω^2	M	ω^2
$10^{15} \text{ g cm}^{-3}$	M_\odot	10^6 s^{-2}	M_\odot	10^6 s^{-2}	M_\odot	10^6 s^{-2}
3.30	1.234	92.8	1.639	112.5	1.913	42.9
3.40	1.236	76.3	1.644	98.2	1.915	24.8
3.50	1.238	60.2	1.647	84.3	1.916	7.0
3.60	1.239	44.4	1.650	70.8	1.916	-10.7
3.70	1.240	29.1	1.652	57.5	1.915	-28.1
3.80	1.240	14.1	1.654	44.7	1.913	-45.5
3.90	1.240	-0.5	1.655	32.1	1.911	-62.6
4.00	1.240	-14.7	1.656	19.9	1.909	-79.6
4.10	1.240	-28.5	1.656	7.9	1.906	-96.5
4.20	1.239	-42.0	1.656	-3.8	1.902	-113.3

TABLE III: Model APR.

	$8\pi\kappa\epsilon_0 = -0.1$		$8\pi\kappa\epsilon_0 = 0$		$8\pi\kappa\epsilon_0 = 0.1$	
ϵ_c	M	ω^2	M	ω^2	M	ω^2
$10^{15} \text{ g cm}^{-3}$	M_\odot	10^6 s^{-2}	M_\odot	10^6 s^{-2}	M_\odot	10^6 s^{-2}
2.00	1.850	186.4	2.134	152.0	2.351	97.1
2.20	1.882	139.1	2.165	104.6	2.371	43.2
2.40	1.902	98.8	2.182	63.8	2.375	-5.0
2.50	1.909	80.8	2.187	45.5	2.373	-27.3
2.60	1.914	64.0	2.190	28.4	2.370	-48.7
2.70	1.917	48.4	2.191	12.3	2.364	-69.2
2.80	1.919	33.8	2.192	-2.7	2.358	-88.8
2.90	1.921	20.2	2.191	-16.9	2.350	-107.8
3.00	1.922	7.4	2.189	-30.2	2.341	-126.2
3.10	1.922	-4.7	2.187	-42.8	2.331	-144.1

TABLE IV: Model BBB2.

	$8\pi\kappa\epsilon_0 = -0.1$		$8\pi\kappa\epsilon_0 = 0$		$8\pi\kappa\epsilon_0 = 0.1$	
ϵ_c	M	ω^2	M	ω^2	M	ω^2
$10^{15} \text{ g cm}^{-3}$	M_\odot	10^6 s^{-2}	M_\odot	10^6 s^{-2}	M_\odot	10^6 s^{-2}
2.30	1.550	143.4	1.880	133.9	2.130	93.8
2.40	1.559	125.1	1.891	116.6	2.139	74.1
2.50	1.567	107.4	1.900	99.8	2.145	55.0
2.60	1.573	90.3	1.907	83.7	2.149	36.3
2.70	1.577	73.8	1.913	68.1	2.152	18.1
2.80	1.580	57.8	1.917	53.2	2.152	0.4
2.90	1.583	42.4	1.919	38.7	2.152	-16.8
3.00	1.584	27.6	1.921	24.8	2.150	-33.5
3.10	1.585	13.3	1.922	11.5	2.147	-49.8
3.20	1.585	-0.5	1.922	-1.4	2.144	-65.7

TABLE V: Model C.

	$8\pi\kappa\epsilon_0 = -0.1$		$8\pi\kappa\epsilon_0 = 0$		$8\pi\kappa\epsilon_0 = 0.1$	
ϵ_c	M	ω^2	M	ω^2	M	ω^2
$10^{15} \text{ g cm}^{-3}$	M_\odot	10^6 s^{-2}	M_\odot	10^6 s^{-2}	M_\odot	10^6 s^{-2}
2.30	1.471	77.8	1.807	89.5	2.069	70.4
2.40	1.477	65.2	1.816	77.9	2.077	57.0
2.50	1.481	52.8	1.822	66.6	2.082	43.7
2.60	1.484	40.6	1.828	55.5	2.086	30.4
2.70	1.486	28.7	1.832	44.6	2.088	17.2
2.80	1.487	17.1	1.835	33.9	2.089	4.1
2.90	1.488	5.7	1.837	23.4	2.089	-9.0
3.00	1.488	-5.5	1.838	13.2	2.088	-22.0
3.10	1.488	-16.5	1.838	3.1	2.085	-35.0
3.20	1.487	-27.2	1.838	-6.7	2.083	-48.0

TABLE VI: Model FPS.

	$8\pi\kappa\epsilon_0 = -0.1$		$8\pi\kappa\epsilon_0 = 0$		$8\pi\kappa\epsilon_0 = 0.1$	
ϵ_c	M	ω^2	M	ω^2	M	ω^2
$10^{15} \text{ g cm}^{-3}$	M_\odot	10^6 s^{-2}	M_\odot	10^6 s^{-2}	M_\odot	10^6 s^{-2}
2.60	1.420	97.3	1.775	104.9	2.039	68.9
2.70	1.425	81.5	1.782	90.5	2.044	52.3
2.80	1.428	66.1	1.787	76.6	2.047	36.0
2.90	1.431	51.2	1.792	63.2	2.049	20.1
3.00	1.433	36.8	1.795	50.1	2.050	4.4
3.10	1.434	22.8	1.797	37.5	2.050	-11.0
3.20	1.434	9.2	1.799	25.3	2.048	-26.2
3.30	1.435	-3.9	1.800	13.4	2.047	-41.1
3.40	1.434	-16.6	1.800	1.9	2.044	-55.9
3.50	1.434	-29.0	1.800	-9.3	2.041	-70.4

TABLE IX: Model WS.

	$8\pi\kappa\epsilon_0 = -0.1$		$8\pi\kappa\epsilon_0 = 0$		$8\pi\kappa\epsilon_0 = 0.1$	
ϵ_c	M	ω^2	M	ω^2	M	ω^2
$10^{15} \text{ g cm}^{-3}$	M_\odot	10^6 s^{-2}	M_\odot	10^6 s^{-2}	M_\odot	10^6 s^{-2}
2.30	1.475	113.9	1.812	118.9	2.072	92.3
2.40	1.481	94.6	1.821	101.6	2.080	74.2
2.50	1.486	76.3	1.828	85.3	2.086	56.8
2.60	1.490	59.0	1.834	69.8	2.090	40.2
2.70	1.492	42.5	1.838	55.1	2.093	24.2
2.80	1.494	26.8	1.841	41.1	2.094	8.8
2.90	1.495	11.8	1.843	27.8	2.094	-6.1
3.00	1.495	-2.5	1.844	15.0	2.093	-20.6
3.10	1.494	-16.2	1.845	2.8	2.091	-34.6
3.20	1.494	-29.3	1.845	-8.9	2.089	-48.2

TABLE VII: Model SLy4.

	$8\pi\kappa\epsilon_0 = -0.1$		$8\pi\kappa\epsilon_0 = 0$		$8\pi\kappa\epsilon_0 = 0.1$	
ϵ_c	M	ω^2	M	ω^2	M	ω^2
$10^{15} \text{ g cm}^{-3}$	M_\odot	10^6 s^{-2}	M_\odot	10^6 s^{-2}	M_\odot	10^6 s^{-2}
2.00	1.692	143.4	1.996	131.5	2.235	99.5
2.10	1.706	124.5	2.011	113.2	2.248	79.1
2.20	1.717	106.6	2.024	95.8	2.257	59.4
2.30	1.725	89.7	2.033	79.2	2.263	40.4
2.40	1.732	73.5	2.040	63.5	2.267	22.1
2.50	1.737	58.2	2.045	48.4	2.268	4.2
2.60	1.740	43.6	2.049	34.1	2.268	-13.0
2.70	1.743	29.8	2.051	20.4	2.266	-29.8
2.80	1.744	16.6	2.052	7.4	2.262	-46.1
2.90	1.744	4.0	2.052	-5.0	2.258	-62.0

TABLE VIII: Model UU.

	$8\pi\kappa\epsilon_0 = -0.1$		$8\pi\kappa\epsilon_0 = 0$		$8\pi\kappa\epsilon_0 = 0.1$	
ϵ_c	M	ω^2	M	ω^2	M	ω^2
$10^{15} \text{ g cm}^{-3}$	M_\odot	10^6 s^{-2}	M_\odot	10^6 s^{-2}	M_\odot	10^6 s^{-2}
2.00	1.843	215.3	2.127	173.0	2.343	110.2
2.20	1.881	166.5	2.163	122.9	2.366	51.8
2.40	1.905	124.2	2.183	79.3	2.372	-0.9
2.60	1.920	87.4	2.193	41.2	2.367	-48.5
2.80	1.928	54.9	2.196	7.8	2.354	-91.9
3.00	1.931	26.2	2.195	-21.7	2.338	-131.5
3.10	1.932	13.0	2.194	-35.2	2.328	-150.1
3.20	1.932	0.5	2.191	-47.9	2.318	-168.0
3.30	1.932	-11.3	2.189	-60.0	2.307	-185.2
3.40	1.932	-22.4	2.186	-71.2	2.296	-201.8

-
- [1] C. M. Will, *Living Rev. Relativity* **9**, 3 (2006).
 - [2] T. Clifton, P. G. Ferreira, A. Padilla, and C. Skordis, *Phys. Rep.* **513**, 1 (2012).
 - [3] M. Bañados and P. G. Ferreira, *Phys. Rev. Lett.* **105**, 011101 (2010).
 - [4] P. Pani, V. Cardoso, and T. Delsate, *Phys. Rev. Lett.* **107**, 031101 (2011).
 - [5] P. Pani, T. Delsate, and V. Cardoso, *Phys. Rev. D* **85**, 084020 (2012).
 - [6] J. Casanellas, P. Pani, I. Lopes, and V. Cardoso, *Astrophys. J.* **745**, 15 (2012).
 - [7] P. P. Avelino, *Phys. Rev. D* **85**, 104053 (2012).
 - [8] S. L. Shapiro and S. A. Teukolsky, *Black Holes, White Dwarfs, and Neutron Stars: The Physics of Compact Objects* (John Wiley and Sons, New York, 1983).
 - [9] S. Chandrasekhar, *Astrophys. J.* **140**, 417 (1964).
 - [10] K. Kokkotas and J. Ruoff, *Astron. Astrophys.* **366**, 565 (2001).
 - [11] S. Weinberg, *Gravitation and Cosmology* (John Wiley & Sons, New York, 1972).
 - [12] J. S. Read, B. D. Lackey, B. J. Owen, and J. L. Friedman, *Phys. Rev. D* **79**, 124032 (2009).
 - [13] P. Haensel and A. Y. Potekhin, *Astron. Astrophys.* **428**, 191 (2004).
 - [14] W. H. Press, S. A. Teukolsky, W. T. Vetterling and B. R. Flannery, *Numerical Recipes in FORTRAN: The Art of Scientific Computing* (Cambridge University Press, Cambridge, 1992).
 - [15] V. Pandharipande, *Nucl. Phys. A* **174**, 641 (1971).
 - [16] A. Akmal, V. R. Pandharipande, and D. G. Ravenhall, *Phys. Rev. C* **58**, 1804 (1998).
 - [17] M. Baldo, I. Bombaci, and G. F. Burgio, *Astron. Astrophys.* **328**, 274 (1997).
 - [18] H. A. Bethe and M. Johnson, *Nucl. Phys. A* **230**, 1 (1974).
 - [19] C. P. Lorenz, D. G. Ravenhall, and C. J. Pethick, *Phys. Rev. Lett.* **70**, 379 (1993).
 - [20] F. Douchin and P. Haensel, *Phys. Lett. B* **485**, 107 (2000).
 - [21] R. B. Wiringa, V. Fiks, and A. Fabrocini, *Phys. Rev. C* **38**, 1010 (1988).
 - [22] J. W. Negele and D. Vautherin, *Nucl. Phys. A* **207**, 298 (1973).
 - [23] P. Demorest, T. Pennucci, S. Ransom, M. Roberts and J. Hessels, *Nature (London)* **467**, 1081 (2010).
 - [24] J. M. Lattimer and M. Prakash, *Phys. Rep.* **442**, 109 (2007).